Topological Imbert-Fedorov Shift in Weyl Semimetals

Qing-Dong Jiang,[1] Hua Jiang,[2] Haiwen Liu,[1,3] Qing-Feng Sun,[1,3,*] and X. C. Xie[1,3,†]

[1]*International Center for Quantum Materials, School of Physics, Peking University, Beijing 100871, People's Republic of China*
[2]*College of Physics, Optoelectronics and Energy, Soochow University, Suzhou 215006, People's Republic of China*
[3]*Collaborative Innovation Center of Quantum Matter, Beijing 100871, People's Republic of China*

The Goos-Hänchen (GH) shift and the Imbert-Fedorov (IF) shift are optical phenomena which describe the longitudinal and transverse lateral shifts at the reflection interface, respectively. Here, we predict the GH and IF shifts in Weyl semimetals (WSMs)—a promising material harboring low energy Weyl fermions, a massless fermionic cousin of photons. Our results show that the GH shift in WSMs is valley independent, which is analogous to that discovered in a 2D relativistic material—graphene. However, the IF shift has never been explored in nonoptical systems, and here we show that it is valley dependent. Furthermore, we find that the IF shift actually originates from the topological effect of the system. Experimentally, the topological IF shift can be utilized to characterize the Weyl semimetals, design valleytronic devices of high efficiency, and measure the Berry curvature.

Introduction.—Modern quantum physics originates from understanding the wave-particle duality of all particles, among which the photon is the first one having been discovered with such a duality. Classically, the physics of a beam of light being reflected at an interface is governed by geometric optics law, where the photons are treated as classical particles. In contrast, when considering the wave nature of photons, spatial shifts at the interface appear as a longitudinal shift in the incident plane [1–3] or a transverse shift normal to the incident plane [4–9], which are known as the Goos-Hänchen (GH) effect and the Imbert-Fedorov (IF) effect, respectively. Because of all particles possessing the wave-particle duality, the spatial shifts are also expected for other particles. For example, the GH effect has been shown to exist in the systems of electrons [10–13], neutrons [14], atoms [15], etc. Particularly for the 2D massless Dirac fermions in graphene systems, the GH shift can be manipulated from positive to negative by tuning an external electric field [16]. However, the IF effect has not been studied in nonoptical systems.

Similar to photons, Weyl particles are also massless. But different from photons, Weyl particles are spin 1/2 chiral fermions and described by the Weyl equation. Recently, Weyl semimetals (WSMs) were proposed as promising systems embedding Weyl fermions, generating intense interest [17–23]. In WSMs, the Weyl nodes always exist in pairs with opposite chiralities, and each Weyl node corresponds to a valley index [24,25]. Several candidates are suggested to be WSMs, including pyrochlore irradiates [17], topological insulator and normal insulator heterostructures [19], staggered flux states in cold atom systems [21], and photonic crystals based on double-gyroid structures [22]. There are two kinds of WSMs: the inversion symmetry broken WSMs and the time reversal symmetry broken WSMs. Very recently, ARPES and transport measurements have shown convincing data on the realization of WSMs in TaAs and related materials, which break the inversion symmetry [26–28]. However, the experimental realization of the time reversal broken WSMs remains a challenge. This failure cannot be ascribed to the impediment of the material growth technique (e.g., $Y_2Ir_2O_7$ [29,30] and $HgCr_2Se_4$ [31,32]), but to the scarcity of the method of direct experimental identification of WSMs [33]. Because of the topological properties of the Weyl fermions, the WSMs may possess exotic wave-packet dynamics, which indicates a new route to characterizing WSMs and potential applications in valleytronics [34–37].

In this Letter, we predict the GH effect and the IF effect for 3D Weyl fermions in WSMs. By using the wave-packet method, we derive analytic results for the spatial shift of the GH effect and the IF effect. Our results show that the GH shift is valley independent. By contrast, the IF shift is valley dependent (see Fig. 1), which gives rise to the valley-dependent anomalous velocities in the system. Because the IF shift is perpendicular to the incident plane, it is a generic 3D effect and could never appear in a 2D material, e.g., the graphene [16]. Furthermore, we demonstrate that the IF shift originates from the topological effect of the system, namely, the Berry curvature of the system. Remarkably, the consequence of the valley-dependent anomalous velocity is significant enough to be detected experimentally. Finally, we discuss three applications of the valley-dependent IF shift: (i) effectively characterizing the WSMs, (ii) directly detecting the Berry curvature, and (iii) efficiently inducing a valley current with a high polarization rate.

Quantum GH and IF effects in WSMs.—The Hamiltonian of the WSMs system is
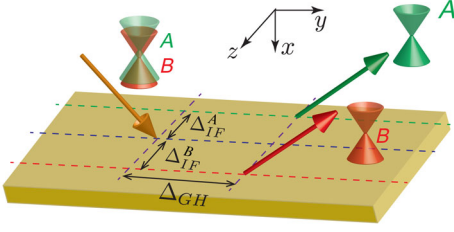
FIG. 1 (color online). Illustration of GH effect and IF effect in WSMs. The orange arrow represents the incident wave packet which includes Weyl fermions from two valleys, whereas the green (red) arrow represents the reflected wave packet of Weyl fermions only from valley A (B). Δ_{GH} denotes the GH shift, and $\Delta_{\mathrm{IF}}^{A(B)}$ stands for the IF shift of valley A (B). This figure shows the positive GH shift case only.

$$\mathcal{H} = \begin{cases} \sum_{i=x,y,z} v_i \hat{p}_i \sigma_i & (x \leq 0) \\ \sum_{i=x,y,z} v_i' \hat{p}_i \sigma_i + V(x) & (x > 0) \end{cases}, \quad (1)$$

where v_i (v_i') is velocity parameter for region $x \leq 0$ ($x > 0$); $\hat{p}_i$ are momentum operators, $V(x)$ is potential, and σ_i stand for Pauli matrices. This Hamiltonian indicates an interface located at $x = 0$ in the WSMs [see Fig. 2(a)]. The effective Hamiltonian (1) can describe both the time reversal symmetry broken WSMs and the inversion symmetry broken WAMs, so the following results are valid for both cases. We consider a beam of Weyl fermions incident from the region $x < 0$ modeled by a Gaussian wave packet as $\psi_g^{\mathrm{in}}(\mathbf{r}) = \int_{-\infty}^{\infty} \int_{-\infty}^{\infty} dk_y dk_z f(k_y - \bar{k}_y) f(k_z - \bar{k}_z) \psi^{\mathrm{in}}(\mathbf{k}, \mathbf{r})$, where $f(k_s - \bar{k}_s) = (\sqrt{2\pi}\Delta_{k_s})^{-1} e^{-(k_s - \bar{k}_s)^2/2\Delta_{k_s}^2}$ are Gaussian distribution functions of width Δ_{k_s} peaked at the mean wave vector $(\bar{k}_x, \bar{k}_y, \bar{k}_z)$, with $s = y, z$. Note that none of our results depend on the shape of the wave packet. Here, $\psi^{\mathrm{in}}(\mathbf{k}, \mathbf{r})$ is the incident wave function, which is a solution of the Weyl equation, i.e., $\mathcal{H}\psi^{\mathrm{in}} = E\psi^{\mathrm{in}}$ for region $x < 0$:

$$\psi^{\mathrm{in}}(\mathbf{k}, \mathbf{r}) = \frac{1}{\sqrt{1 + \eta^2}} \begin{pmatrix} e^{-i\alpha/2} \\ \eta e^{i\alpha/2} \end{pmatrix} e^{ik_x x + ik_y y + ik_z z}, \quad (2)$$

where $k_x = \sqrt{E^2 - (\hbar v_y k_y)^2 - (\hbar v_z k_z)^2}/\hbar v_x$, $\alpha = \tan^{-1}(v_y k_y/v_x k_x)$, and $\eta = \sqrt{(E - \hbar v_z k_z)/(E + \hbar v_z k_z)}$. Analogously, the reflected wave packet can be written as $\psi_g^{\mathrm{re}}(\mathbf{r}) = \int_{-\infty}^{\infty} \int_{-\infty}^{\infty} dk_y dk_z f(k_y - \bar{k}_y) f(k_z - \bar{k}_z) \psi^{\mathrm{re}}(\mathbf{k}, \mathbf{r})$, where ψ^{re} is the reflected wave function. ψ^{re} can be obtained from the incident wave Eq. (2) by the substitution $k_x \mapsto -k_x$, $\alpha \mapsto \pi - \alpha$ and multiplication by the reflection amplitude $r = |r| e^{i\phi_r}$. The integrals of ψ_g^{in} and ψ_g^{re} give the center of the wave packets, and therefore we can obtain the spatial shifts in the y, z directions [38]:

$$\Delta_{\pm}^y = -\frac{\partial}{\partial k_y} \phi_r(\bar{k}_y, \bar{k}_z) \mp \frac{\partial}{\partial k_y} \alpha(\bar{k}_y, \bar{k}_z)$$

$$\Delta_{\pm}^z = -\frac{\partial}{\partial k_z} \phi_r(\bar{k}_y, \bar{k}_z) \mp \frac{\partial}{\partial k_z} \alpha(\bar{k}_y, \bar{k}_z). \quad (3)$$

The spatial shifts for Weyl fermions are defined as the average shifts of the two spinor components: $\Delta^{y(z)} = (\Delta_+^{y(z)} + \eta^2 \Delta_-^{y(z)})/(1 + \eta^2)$. In Eq. (3), $\alpha(\bar{k}_y, \bar{k}_z)$ represents the incident angle, and ϕ_r is the phase of the reflection coefficient, which can be obtained by matching the wave function at $x = 0$. If the incident wave packet is confined in the x-y plane, the in-plane shift Δ^y and the out-of-plane shift Δ^z of the wave packet corresponds to the GH shift Δ_{GH} and the IF shift Δ_{IF}:

$$\Delta_{\mathrm{GH}} = \frac{v_y'}{v_x'} \frac{(1 + \beta\sin^2\bar{\alpha} - \frac{V}{E})}{\beta \sin\bar{\alpha}\cos\bar{\alpha}\kappa}, \quad (4)$$

$$\Delta_{\mathrm{IF}} = -C \left| \frac{\hbar v_x v_z}{v_y} \right| \frac{1}{E\tan\theta} \left[\frac{1 - \frac{E}{V}(1 - \gamma)}{1 - \frac{E}{V}(1 - \beta)} \right], \quad (5)$$

where $\kappa = \sqrt{(\hbar v_y' k_y)^2 + (\hbar v_z' k_z)^2 - (E - V)^2}/\hbar v_x'$, $\beta = v_y'/v_y$, $\gamma = v_z'/v_z$, $\bar{\alpha} = \tan^{-1}(v_y \bar{k}_y/v_x \bar{k}_x)$, and $\theta = \tan^{-1}(\bar{k}_y/\bar{k}_x)$. $C \equiv \mathrm{sgn}[v_x v_y v_z]$ is the chirality of the valley in WSMs. From Eq. (5), one sees that the IF shift is very large when the Fermi energy E is close to the Weyl nodes at zero. Moreover, the IF shift remains at a large value when E is not far away from the Weyl node.

We take the incident Fermi energy $E = 100$ meV, potential $V = 150$ meV, and velocities $v_i = v_i' = 10^6$ m/s, where $i = x, y, z$. In this case, $\beta = \gamma = 1$. Note that the two valleys (A, B) of a WSM have opposite chiralities. Figure 2(b) shows the spatial shifts versus the incident angle θ, where both the GH and IF shifts are odd functions of the incident angle, which is consistent with symmetry analysis. Figure 2(c) shows the valley independence and potential dependence of GH shift Δ_{GH}, which can be tuned from positive to negative by external field V. This feature is analogous to the GH shift in graphene [16]. Figure 2(d) illustrates that the IF shift is independent of potential, but that it depends on valley index. The IF shift can be utilized to manipulate the valley degree of freedom.

Topological origin of the IF effect.—Based on the semiclassical dynamics of the wave packet, we show that the IF shift is closely related to the Berry curvature of the system. Let us assume the velocity $v_i = v_i'$ ($i = x, y, z$) in the WSM system. In this case, $\beta = \gamma = 1$, and Eq. (5) reduces to $\Delta_{\mathrm{IF}} = -(\hbar v_x v_z/v_y)(1/E\tan\theta)$. Commonly, the Weyl node can be regarded as a magnetic monopole in k space [39] and thereby generates an effective magnetic field in k space. The Berry curvature of Hamiltonian equation (1) in region $(x \leq 0)$ is $\Omega^{\pm} = \mp(\hbar^3 v_x v_y v_z \mathbf{k}/2E^3)$ for the conduction band and the valence band [40], respectively.
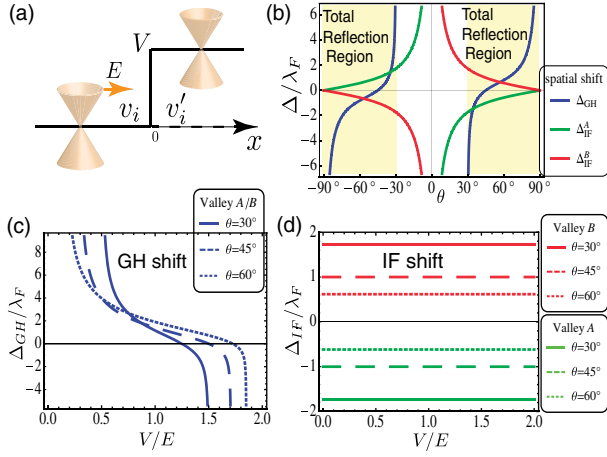
FIG. 2 (color online). (a) Schematic of a p-n junction with an interface at $x = 0$. v_i (v_i') is the velocity in the left (right) side of the interface. E is the Fermi energy, and V is the potential difference of the junction. (b) GH shift Δ_{GH} and IF shift $\Delta_{\mathrm{IF}}^{A(B)}$ of valley A (B) versus incident angle θ. Total reflection happens at $\theta \geq 30°$ (the yellow shaded region). $\lambda_F = hv_i/E$ stands for the wavelength of the Weyl fermions. (c) Potential dependence of the GH shift for incident angle $\theta = 30°$ (solid line), $45°$ (dashed line), and $60°$ (dotted line). (d) Potential dependence of the IF shift for incident angle $\theta = 30°$ (solid lines), $45°$ (dashed lines), and $60°$ (dotted lines).

The semiclassical equation of motion [40,41] of the wave packet is $(d\mathbf{r}/dt) = (\partial E(\mathbf{k})/\hbar\partial\mathbf{k}) - (d\mathbf{k}/dt) \times \Omega$, where $\mathbf{r}$ and $\mathbf{k}$ are the center positions of the wave packet in phase space. We assume that the incident wave packet locates in the conduction band, and we consider the incident wave packet in the x-y plane with $k_z = 0$. The variation of k_x by potential V and nonzero Berry curvature Ω_y leads to the IF shift Δ_{IF} in the z direction:

$$\Delta_{\mathrm{IF}} = -\int_{k_x}^{-k_x} dk_x \Omega_y = -\left(\frac{\hbar v_x v_z}{v_y}\right)\frac{1}{E\tan\theta}, \quad (6)$$

where $\tan\theta = k_y/k_x$. Remarkably, Eqs. (6) and (5) completely coincide in the case of $\beta = \gamma$. This coincidence does not depend on linear dispersion of the system [38]. The consistency between Berry curvature calculations and wave-packet results strongly support the conclusion that the IF shift is mainly a topological effect. The IF shift in WSMs is quite different from that in optical systems. Specifically, Δ_{IF} reaches the maximum in WSMs [see Fig. 2(b)] when comparing the zero value in optical systems at $\theta = 0°$ [6,8]. This is because the conservation of k_y, k_z guarantees that the Weyl Fermions stay in the same valley during the reflection processes in WSMs. In contrast, the polarization of the photons changes during the reflection processes, which will severely influence Δ_{IF}. In the Supplemental Material [38], we present the comparison between the IF shift in WSMs and in various spin Hall effects. However, the semiclassical equation cannot be

generally applied to all cases of the reflection process because of the breakdown of the adiabatic approximation for some systems.

Anomalous velocities induced by the IF effect.—We consider a well collimated beam of Weyl fermions propagating in the middle layer (region II) of a sandwich structure, which is constructed by three layers of WSMs [see Fig. 3(a)]. The applied electric potential profile is shown below the sandwich structure. The height of the structure is h and the width of region II is d. There are both GH and IF shifts at the two interfaces ($x = \pm(d/2)$). In order to observe the valley-dependent IF shift, the mirror symmetry at about the $x = 0$ plane needs to be broken [38]. Thus, we consider that the z direction velocities in the three regions are different, with $v_z^{\mathrm{I}} = v_L$, $v_z^{\mathrm{II}} = v$, and $v_z^{\mathrm{III}} = v_R$, whereas the x and y direction velocities are still identical, $v_{x/y}^{\mathrm{I}} = v_{x/y}^{\mathrm{II}} = v_{x/y}^{\mathrm{III}} = v$. Without considering the spatial shifts at the interfaces, the normal velocities in region II in the y and z directions are $v_{n,y} = v\sin\theta\cos\phi$ and $v_{n,z} = v\sin\theta\sin\phi$, where angles θ and ϕ characterize the incident direction of the wave packet [see Fig. 3(b)]. We denote the GH and IF shifts at the left (right) interface as $\Delta_{\mathrm{GH}}^{L(R)}$ and $\Delta_{\mathrm{IF}}^{L(R)}$, respectively. During multiple reflections in region II, the GH and IF shifts are accumulated, and they induce average anomalous velocities:
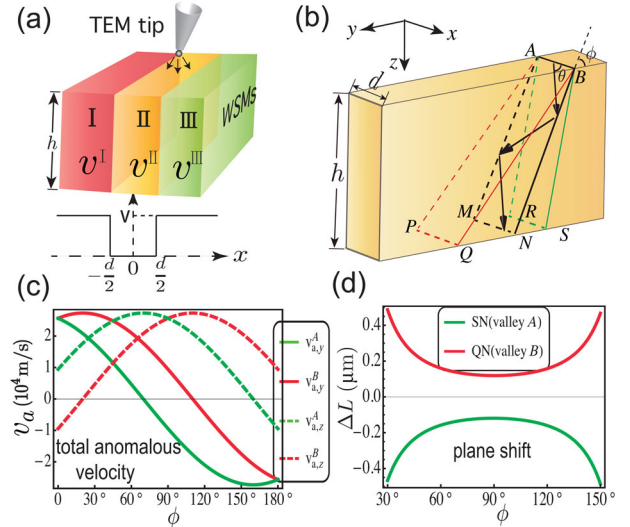
FIG. 3 (color online). (a) Schematic of the valley splitter for Weyl fermions. Regions I, II, and III are three WSM layers with different velocities $\mathbf{v}^{\mathrm{I}}$, $\mathbf{v}^{\mathrm{II}}$, and $\mathbf{v}^{\mathrm{III}}$. (b) Illustration of the wave-packet trajectory (the black arrow) of Weyl fermions in region II. The electrons are injected by a TEM tip with incident polar angle θ and azimuthal angle ϕ. The parameter θ is fixed at $50°$ in our calculation. In an ordinary case, the trajectory of a wave packet stays in the $ABMN$ plane. However, due to the valley-dependent IF shift, the trajectory of Weyl fermions from valley A (B) would shift to the plane $ABRS$ ($ABPQ$). (c) ϕ dependence of the total anomalous velocities. (d) The propagating plane shift for two valleys. After considering the IF shift, SN (QN) is the final position shift for valley A (B).

$v_{a,y} = [(\Delta_{GH}^L + \Delta_{GH}^R)\cos\phi + (\Delta_{IF}^L + \Delta_{IF}^R)\sin\phi]/(2\Delta t)$ and $v_{a,z} = [(\Delta_{GH}^L + \Delta_{GH}^R)\sin\phi + (\Delta_{IF}^L + \Delta_{IF}^R)\cos\phi]/(2\Delta t)$. $\Delta t = d/(v\cos\theta)$ represents the propagating time between two subsequent reflections. Therefore, the normal and anomalous velocities result in the total velocity: $v_{t,y(z)} = v_{n,y(z)} + v_{a,y(z)}$.

We set the parameters $E = 100$ meV, $V = 150$ meV, $h = 10\,\mu$m, $d = 50$ nm, $v_z^I = v_L = 1.2 \times 10^6$ m/s, $v_z^{II} = v = 10^6$ m/s, $v_z^{III} = v_R = 0.8 \times 10^6$ m/s, and velocities in other directions are all set to 10^6 m/s [42]. Figure 3(c) shows ϕ the dependence of the total anomalous velocities induced by the spatial shifts. The anomalous velocities are valley dependent, which implies that the total velocities also depend on the valley index. Eventually, the different velocities of the two valleys lead to macroscopic separation in real space, which is experimentally detectable. Figure 3(d) shows the opposite position shift at the bottom of region II for valley A and valley B. A GH shift cannot induce the position shift, because the GH shift always lies in the propagating plane. In contrast, an IF shift can induce the position shifts (of micrometer order) for two valleys (**SN** and **QN**) [38].

Identification of WSMs.—The experimental observation of time reversal broken-type WSMs has not appeared, mainly due to the lack of an efficient detection method [43–45]. The direct ARPES measurements of energy dispersions are currently scant due to the constraint of magnetic properties of WSMs. Here, we suggest that the IF effect can be used as an experimental identification of WSMs. It has been shown that the topological IF shift splits the incident wave packets into opposite directions with respect to the valley index. Thus, the splitting of wave packets on the bottom of region II in Fig. 3(a) can serve as a hallmark of WSMs. Furthermore, even considering an incident wave packet with a finite angle range, this exotic splitting can also exist.

Pure valley polarization.—Let us consider a TEM injector with incident angle range δ ($\theta \in [\theta_c - \delta/2, \theta_c + \delta/2]$ and $\phi \in [\phi_c - \delta/2, \phi_c + \delta/2]$) at the top of region II, and study the valley density distribution at the bottom [see Fig. 4(d)]. We calculate the valley density distribution with parameters $E = 100$ meV, $V = 150$ meV, $h = 10\,\mu$m, $d = 80$ nm, $\delta = 3°$, $\theta_c = 32.5°$, and $\phi_c = 90°$. Without considering anomalous velocities, the density distributions for valleys A and B are maximized at the center of the y direction, and thus they are not distinguishable [38]. In contrast, after considering the anomalous velocities, Figs. 4(a), 4(b), and 4(c) show the density distributions for valley A, valley B, and both valley A and valley B, respectively. The IF effect induces opposite shifts in the y direction for valley A and valley B. Since the Weyl fermions from valleys A and B are well separated in the space of micrometer order, pure valley current can be generated in the green (red) region [see Fig. 4(c)]. This schematic setup in Fig. 4(d) can be utilized to generate pure valley current.
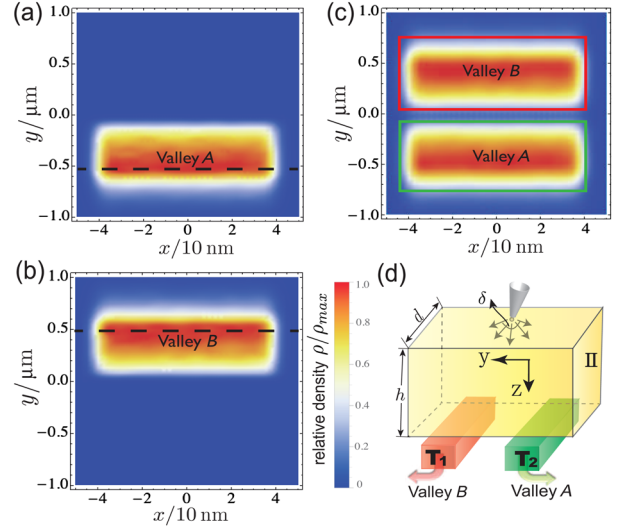
FIG. 4 (color online).   Valley density distribution shift caused by the IF effect. (a), (b), and (c) show the relative density distribution of valley A, valley B, and both, respectively, after considering the GH and IF effects. The color bar on the right represents the relative density ρ/ρ_{max} of Weyl fermions. Here, ρ (ρ_{max}) represents the absolute (maximum) density of the Weyl fermions at the bottom. The dashed lines indicate the location of the maximum intensity of density. The red (green) box in (c) guides the eye to the region where only valley B (A) exists (pure valley polarization). (d) Proposed setup for generating valley current. The devices T_1 (red) and T_2 (green) are two terminals which can extract the valley current out.

Detection of Berry curvature.—The Berry curvature, a gauge invariant quantity, should be detectable in experiments [40]. However, to date, there has not been a feasible experimental method to measure the Berry curvature in real materials. The topological IF effect provides a new way to measure the Berry curvature. For a system with inversion symmetry, the Berry curvature is an even function of wave vector $\mathbf{k}$, i.e., $\Omega(\mathbf{k}) = \Omega(-\mathbf{k})$ [40], which is usually satisfied in WSMs [17–19]. Considering a wave packet propagating in the x-y plane with $k_z = 0$, the IF shift can be expressed as $\Delta_{IF} = 2\int_0^{k_x} dk_x \Omega_y(\mathbf{k})$, or

$$\Omega_y(\mathbf{k}) = \frac{1}{2}\frac{\partial\Delta_{IF}(\mathbf{k})}{\partial k_x}. \qquad (7)$$

To measure the Berry curvature Ω_y, one needs to collect the IF shift in the z direction $\Delta_{IF}(E,\theta)$ as a function of energy E and incidence angle θ. The $\Delta_{IF}(E,\theta)$ can be transformed into $\Delta_{IF}(k_x, k_y)$, and its derivative produces the Berry curvature $\Omega_y(\mathbf{k})$. In the same way, the IF shift in other directions can be used to obtain $\Omega_x(\mathbf{k})$ and $\Omega_z(\mathbf{k})$.

Summary.—We obtained analytical expressions of the GH shift and IF shift at the interface of WSMs. We demonstrated that the IF shift is valley dependent, and that it can be attributed to the topological nature of the system. This IF shift can lead to valley-dependent

anomalous velocity, which is experimentally detectable. Finally, we discussed three applications of the topological IF shift, including characterization of WSMs, fabrication of highly efficient valleytronic devices, and detection of the Berry curvature.

Q.-D. J., H. J., and H. L. contributed equally to this work.

*sunqf@pku.edu.cn
†xcxie@pku.edu.cn

[1] F. Goos and H. Hächen, Ann. Phys. (Berlin) **436**, 333 (1947).
[2] F. Bretenaker, A. Le Floch, and L. Dutriaux, Phys. Rev. Lett. **68**, 931 (1992).
[3] M. Peccianti, A. Dyadyusha, M. Kaczmarek, and G. Assanto, Nat. Phys. **2**, 737 (2006).
[4] F. I. Fedorov, Dokl. Akad. Nauk SSSR **105**, 465 (1955).
[5] C. Imbert, Phys. Rev. D **5**, 787 (1972).
[6] M. Onoda, S. Murakami, and N. Nagaosa, Phys. Rev. Lett. **93**, 083901 (2004).
[7] K. Y. Bliokh and Y. P. Bliokh, Phys. Rev. Lett. **96**, 073903 (2006); K. Y. Bliokh, A. Niv, V. Kleiner, and E. Hasman, Nat. Photonics **2**, 748 (2008).
[8] O. Hosten and P. Kwiat, Science **319**, 787 (2008).
[9] X. Yin, Z. Ye, J. Rho, Y. Wang, and X. Zhang, Science **339**, 1405 (2013).
[10] S. C. Miller, Jr. and N. Ashby, Phys. Rev. Lett. **29**, 740 (1972).
[11] D. M. Fradkin and R. J. Kashuba, Phys. Rev. D **9**, 2775 (1974).
[12] X. Chen, X.-J. Lu, Y. Ban, and C.-F. Li, J. Opt. **15**, 033001 (2013).
[13] Z. Wu, F. Zhai, F. M. Peeters, H. Q. Xu, and K. Chang, Phys. Rev. Lett. **106**, 176802 (2011).
[14] V.-O. de Haan, J. Plomp, T. M. Rekveldt, W. H. Kraan, and A. A. van Well, Phys. Rev. Lett. **104**, 010401 (2010).
[15] J. Huang, Z. Duan, H. Y. Ling, and W. Zhang, Phys. Rev. A **77**, 063608 (2008).
[16] C. W. J. Beenakker, R. A. Sepkhanov, A. R. Akhmerov, and J. Tworzydło, Phys. Rev. Lett. **102**, 146804 (2009).
[17] X. Wan, A. M. Turner, A. Vishwanath, and S. Y. Savrasov, Phys. Rev. B **83**, 205101 (2011).
[18] G. Xu, H. Weng, Z. Wang, X. Dai, and Z. Fang, Phys. Rev. Lett. **107**, 186806 (2011).
[19] A. A. Burkov and L. Balents, Phys. Rev. Lett. **107**, 127205 (2011).
[20] P. Hosur, S. A. Parameswaran, and A. Vishwanath, Phys. Rev. Lett. **108**, 046602 (2012).
[21] J.-H. Jiang, Phys. Rev. A **85**, 033640 (2012).
[22] L. Lu, L. Fu, J. D. Joannopoulos, and M. Soljačić, Nat. Photonics **7**, 294 (2013).
[23] S. A. Yang, H. Pan, and F. Zhang, Phys. Rev. Lett. **113**, 046401 (2014).
[24] H. B. Nielsen and M. Ninomiya, Nucl. Phys. **B185**, 20 (1981).
[25] H. B. Nielsen and M. Ninomiya, Phys. Lett. **130B**, 389 (1983).
[26] H. Weng, C. Fang, Z. Fang, B. A. Bernevig, and X. Dai, Phys. Rev. X **5**, 011029 (2015); S.-M. Huang *et al.*, Nat. Commun. **6**, 7373 (2015).
[27] S.-Y. Xu *et al.*, Science **349**, 613 (2015); B. Q. Lv *et al.*, Phys. Rev. X **5**, 031013 (2015); Nat. Phys., DOI: 10.1038/nphys3426 (2015).
[28] X. Huang *et al.*, arXiv:1503.01304; C. Zhang *et al.*, arXiv:1504.07698.
[29] D. Yanagishima and Y. Maeno, J. Phys. Soc. Jpn. **70**, 2880 (2001).
[30] S. T. Bramwell and M. J. P. Gingras, Science **294**, 1495 (2001).
[31] H. W. Lehmann and F. P. Emmenegger, Solid State Commun. **7**, 965 (1969).
[32] T. Guan *et al.*, Phys. Rev. Lett. **115**, 087002 (2015).
[33] P. Hosur and X.-L. Qi, C.R. Phys. **14**, 857 (2013).
[34] A, Rycerz, J. Tworzydło, and C. W. J. Beenakker, Nat. Phys. **3**, 172 (2007).
[35] D. Xiao, W. Yao, and Q. Niu, Phys. Rev. Lett. **99**, 236809 (2007).
[36] K. F. Mak, K. L. McGill, J. Park, and P. L. McEuen, Science **344**, 1489 (2014).
[37] R. V. Gorbachev, J. C. W. Song, G. L. Yu, A. V. Kretinin, F. Withers, Y. Cao, A. Mishchenko, I. V. Grigorieva, K. S. Novoselov, L. S. Levitov, and A. K. Geim, Science **346**, 448 (2014).
[38] See Supplemental Material at http://link.aps.org/supplemental/10.1103/PhysRevLett.115.156602 for more details.
[39] Z. Fang, N. Nagaosa, K. S. Takahashi, A. Asamitsu, R. Mathieu, T. Ogasawara, H. Yamada, M. Kawasaki, Y. Tokura, and K. Terakura, Science **302**, 92 (2003).
[40] D. Xiao, M.-C. Chang, and Q. Niu, Rev. Mod. Phys. **82**, 1959 (2010).
[41] M.-C. Chang and Q. Niu, Phys. Rev. B **53**, 7010 (1996).
[42] Note that the velocity parameters are closely related to the hopping parameters, which can be tuned by a strain on the bulk materials. See Ref. [37] for details.
[43] V. Aji, Phys. Rev. B **85**, 241101 (2012).
[44] D. T. Son and B. Z. Spivak, Phys. Rev. B **88**, 104412 (2013).
[45] S. A. Parameswaran, T. Grover, D. A. Abanin, D. A. Pesin, and A. Vishwanath, Phys. Rev. X **4**, 031035 (2014).